Geological Society of America
Special Paper 365
2002

Stratigraphic record of Pleistocene initiation and slip on the Coyote Creek fault, Lower Coyote Creek, southern California

Rebecca J. Dorsey*
Department of Geological Sciences, 1272 University of Oregon, Eugene, Oregon 97403-1272, USA

ABSTRACT

The Coyote Creek fault is a major strand of the San Jacinto fault zone in southern California. Pleistocene sediments and sedimentary rocks exposed in the lower Coyote Creek area preserve a record of surface deformation, stream reorganization, and erosion that resulted from initiation and slip on the Coyote Badlands strand of the Coyote Creek fault. A well-exposed section of conglomerate and sandstone contains the 760 ka Bishop Ash and reveals (1) complete reversal of paleocurrents from northwest-directed (opposed to modern drainages) to southeast-directed (consistent with modern drainages); (2) fanning dips and a progressive unconformity bounded by the Coyote Creek and Box Canyon faults; (3) a thick gravel unit (Qg) that caps the fanning-dip section and accumulated between ca. 700 and 600 ka; and (4) post-Qg offset and deep erosion of the entire section. The fanning dips and reversal of paleocurrents are interpreted to record initiation of the Box Canyon and Coyote Creek faults by dip-slip (normal) displacement beginning at 750 ka. Strike-slip offset of Qg is equal to total offset on the Coyote Creek fault in the study area (~6 km), indicating that strike-slip motion on the fault began after deposition of Qg, after ca. 600 ± 100 ka. This gives a time-averaged slip rate in Coyote Creek of ~10 mm/yr. Two alternative models for Pleistocene fault evolution are considered: (1) prior to ca. 600 ka, the Clark and southern Coyote Creek faults were connected via a releasing bend that produced a pull-apart basin in the Borrego Badlands, and initiation of the Coyote Badlands strand at 600 ka represents northwestward propagation of the Coyote Creek fault; or (2) the Coyote Creek fault was initiated along most or all of its length at ca. 600 ka, establishing the modern link to plate-boundary faults in the Imperial Valley. Existing data are equivocal on this question.

INTRODUCTION

The San Jacinto fault zone is a seismically active system of strike-slip fault segments, segment-bounding discontinuities, and related zones of contractional and extensional deformation in southern California (Sharp, 1967; Wesnousky, 1986, 1988; Sanders, 1989; Sanders and Magistrale, 1997). The San Jacinto splays off from the San Andreas fault in a complex zone of diffuse strike-slip faults northwest of San Bernardino (Fig. 1; Matti et al., 1992; Morton and Matti, 1993), and southeast of there the two fault zones accommodate most of the motion on the Pacific-North American plate boundary (Fig. 1; DeMets et al., 1994; DeMets, 1995). Although recent studies of historical seismicity provide insights into modern fault behavior and interactions, relatively little is known about the Pleistocene history of fault slip, sedimentation, and deformation in the San Jacinto fault zone. The evolution of the fault zone at geologic time scales of 0.5–2.0 Ma has been largely overlooked in

*E-mail: rdorsey@darkwing.uoregon.edu

Dorsey, R.J., 2002, Stratigraphic record of Pleistocene initiation and slip on the Coyote Creek fault, Lower Coyote Creek, southern California, *in* Barth, A., ed., Contributions to Crustal Evolution of the Southwestern United States: Boulder, Colorado, Geological Society of America Special Paper 365, p. 251–269.

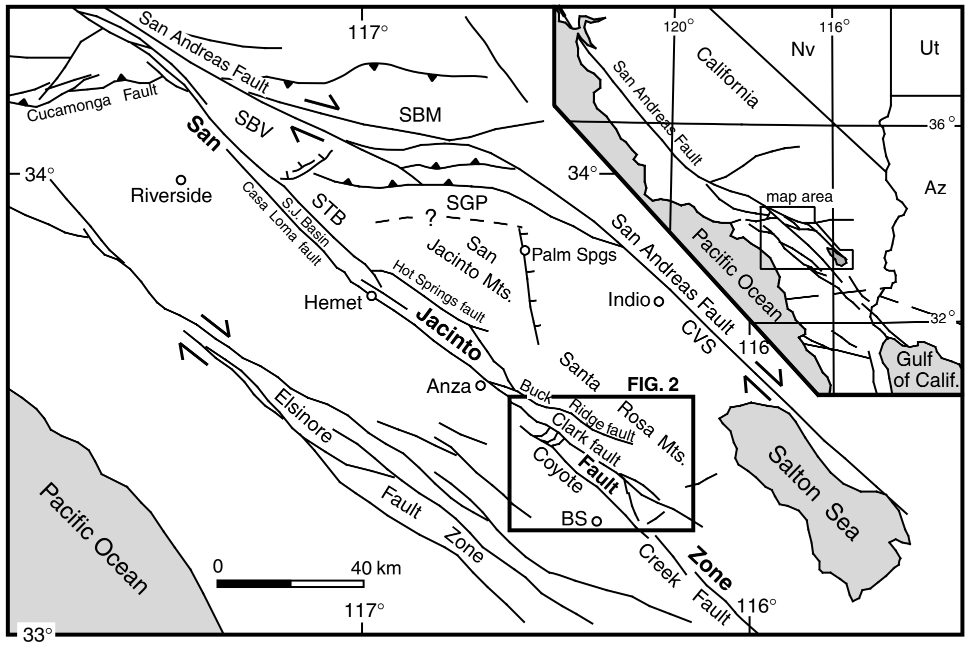

Figure 1. Map showing the San Andreas, San Jacinto, and Elsinore strike-slip fault zones in southern California, and location of Figure 2. BS—Borrego Springs, CVS—Coachella Valley strand of San Andreas fault, SBM—San Bernardino Mountains, SBV—San Bernardino Valley, SGP—San Gorgonio Pass, S.J. Basin—San Jacinto basin, STB—San Timoteo Badlands. Modified from Sharp (1967).

previous studies, in spite of its significance for understanding the fault kinematics, strain partitioning, and regional slip budget of the San Andreas fault system.

One poorly understood aspect of the San Jacinto fault zone is its age of initiation, which is directly related to long-term slip rate. Based on velocities determined from GPS measurements and offset of late Quaternary deposits, it is generally believed that slip on the San Jacinto fault is ~10–12 mm/yr and slip on the San Andreas fault southeast of the Transverse Ranges (Coachella Valley strand) is ~25 mm/yr (Sharp, 1981; Rockwell et al., 1990; Bennett et al., 1996; Kendrick et al., 1994). Northwest of Cajon Pass, slip on the San Jacinto and San Andreas faults merge to produce ~35 mm/yr slip on the Mojave segment of the San Andreas fault (Weldon and Sieh, 1985; Weldon and Humphreys, 1986; Humphreys and Weldon, 1994). If one assumes a rate of 10 mm/yr and total offset of 24 km (Sharp, 1967), the age of inception for the San Jacinto fault zone is inferred to be ca. 2.4 Ma. However, geologic and stratigraphic relationships in the northern part of the fault zone provide evidence for initiation between ca. 1.5 and 1.0 Ma (Morton and Matti, 1993; Albright, 1999), which would imply a slip rate of ~16–24 mm/yr. These discrepancies reflect existing limits in our understanding of the fault zone, and indicate a need for detailed studies of fault initiation and evolution in areas where stratigraphic controls exist.

This paper presents a stratigraphic analysis of middle Pleistocene sediments and sedimentary rocks exposed in the central San Jacinto fault zone north of Borrego Springs, California (Figs. 1, 2). Internal stratigraphy, lithofacies, paleocurrent data, and growth structures in these strata provide a record of sedimentation and surface deformation that resulted from initiation and slip on the Coyote Badlands strand of the Coyote Creek fault, a major strand of the San Jacinto fault zone. The deposits are well exposed in steep gullies and badlands erosional topography, and their age (early to middle Pleistocene) is known from the presence of dated volcanic ashes. Following accumulation of the thick section (~400 m), the sediments have been offset by younger faults and deeply dissected by vigorous erosion. Thus, the area has experienced profound changes in topography over the past 700,000 yr that are clearly related to active strike-slip faulting. In this paper, stratigraphic data are integrated with structural and geomorphic analyses to reconstruct the Pleistocene history of initiation and slip on the Coyote Creek fault in the lower Coyote Creek area.

STRUCTURAL AND GEOMORPHIC SETTING

The two active segments of the San Jacinto fault zone in the study area are the Coyote Creek and Clark faults (Figs. 1, 2). The Clark fault displays abundant geomorphic features characteristic of active strike-slip faulting, such as offset stream channels, beheaded alluvial fans, shutter ridges, and fresh fault scarps cut through late Pleistocene deposits. The Clark fault terminates to the southeast in a zone of diffuse faulting and strongly folded Pleistocene sedimentary rocks at the south end of the Santa Rosa Mountains (Fig. 2; Dibblee, 1954). This is the site of a 1954 M 6.2 earthquake that initiated at the southeast end of the fault and propagated southeastward into the zone of diffuse brittle deformation (Sanders, 1989). Active fault features are extremely well developed along the Clark fault and are also present, but less pronounced, along the trace of the Coyote Creek fault.

This study focuses on a segment of the Coyote Creek fault located between the Borrego Badlands and Fig Tree Valley

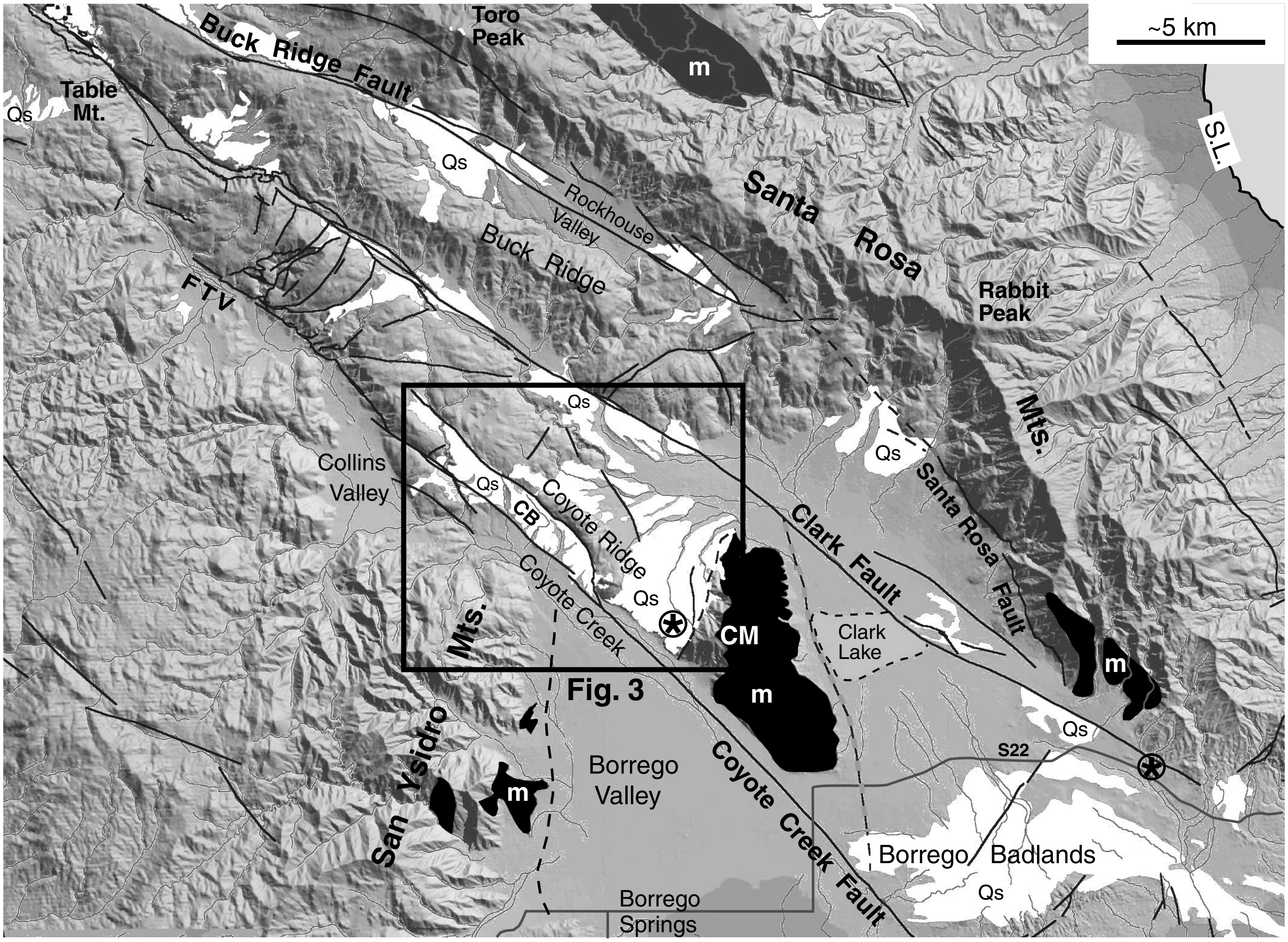

Figure 2. Shaded relief map showing major faults and fault-related topography in the central San Jacinto fault zone. White areas (Qs) are Quaternary sediments and sedimentary rocks; dark areas (m) are Cretaceous Santa Rosa mylonite. Unlabeled areas are mostly nonmylonitic crystalline rocks (rough topography) or late Pleistocene to Quaternary alluvium (low smooth topography); area south of Qs in Borrego Badlands is underlain by sedimentary rocks. Faults are indicated by solid lines, dashed where buried or inferred (except line around Clark Lake). Circled asterisk near southeast end of Clark fault shows location of 1954 M_L-6.2 Arroyo Salada earthquake; asterisk west of Coyote Mountain is the 1969 M_L-5.8 Coyote Mountain earthquake (Sanders, 1989). CB—Coyote Badlands, CM—Coyote Mountain, FTV—Fig Tree Valley, S22—State Highway 22, S.L.—sea level.

(Figs. 2, 3), informally named the Coyote Badlands strand. Displacement on the Coyote Creek fault decreases to the northwest through Fig Tree Valley, and slip is transferred from there to the northeast through a series of normal faults to the Clark fault (Fig. 2; Sharp, 1975). The Buck Ridge fault has measurable offset near Anza (Fig. 1; Sharp, 1967), but observations made during this study show that it has no geologic offset or geomorphic expression where it has been mapped in southeastern Rockhouse Valley (Fig. 2). Thus, it appears that slip on the northwestern part of the Buck Ridge fault either steps south to the Clark fault or is transferred southeast to the Santa Rosa fault south of Toro Peak, or both.

The Santa Rosa fault is a large normal fault that forms a steep topographic escarpment separating the high Santa Rosa Mountains from Clark Valley (Fig. 2). This fault was originally recognized by Dibblee (1954), but Sharp (1967) stated that there is no evidence for a large-offset fault at this location. In fact, numerous features reveal the presence of a large normal fault, including well-preserved high triangular facets defining a linear range front, intense brittle fracture and cataclasis in a steeply southwest-dipping fault zone, short steep drainages and wineglass canyons in the footwall, and asymmetric topography in the Santa Rosa Mountains that reflects tilting to the northeast (Fig. 2). Correlation of bedrock mylonite across the Santa Rosa fault suggests ~400 m of dip-slip separation near its south end, with vertical displacement probably increasing to the north. The largest well-preserved facets along the Santa Rosa range front are 400–500 m high, which can be inferred to represent a

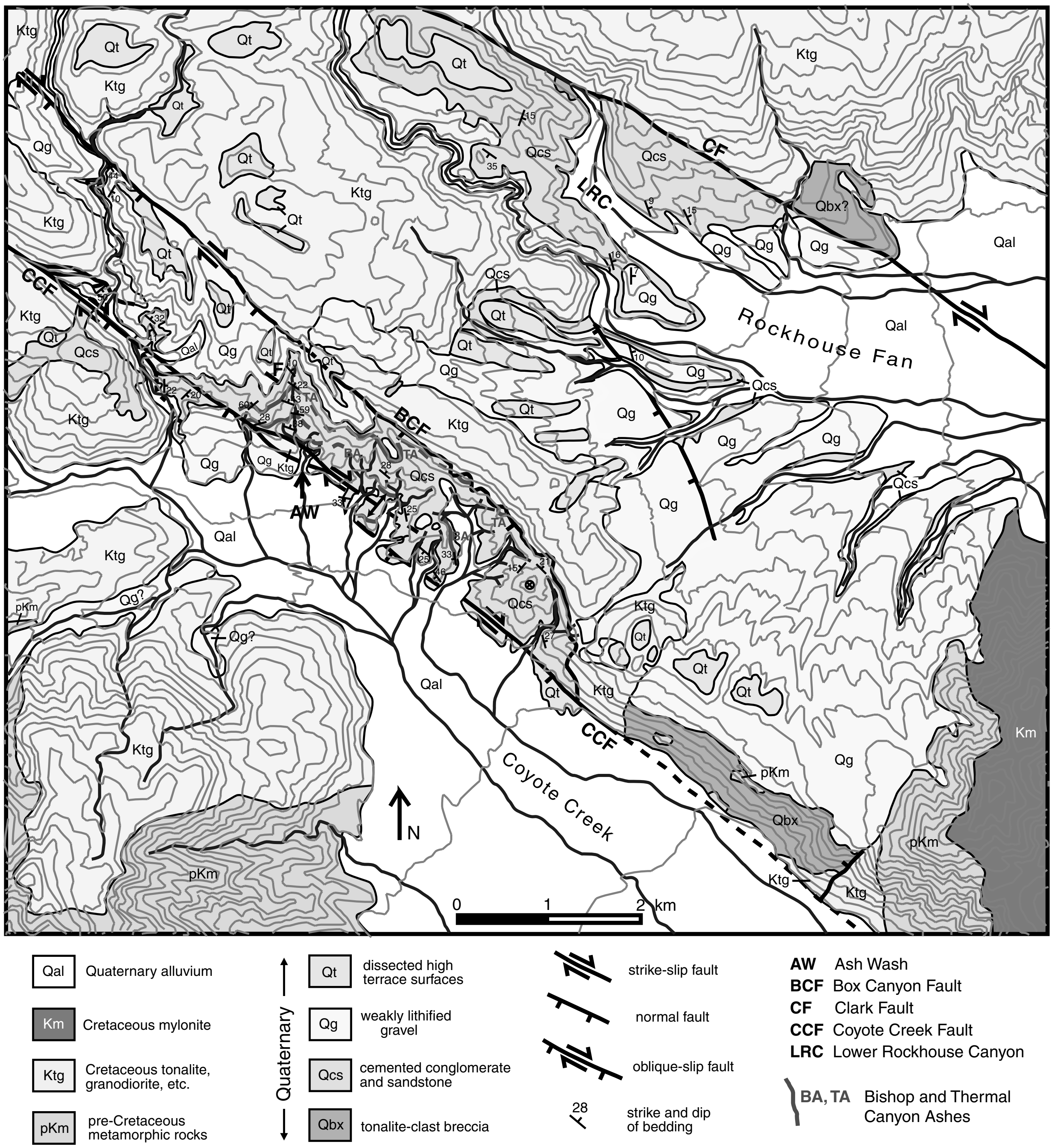

Figure 3. Geologic map of the lower Coyote Creek area. Coyote Badlands is the area of eroding Qcs (sedimentary rocks) and Qg (gravel) bounded by the Box Canyon and Coyote Creek faults. Thin gray lines are topographic contours, contour interval 40 m. Line "F" shows position and orientation of fulcrum of tilting (neutral line) as determined for fanning-dip growth structure in Figure 9. Most contacts within crystalline rocks (pKm, Ktg, Km) are from Sharp (1967).

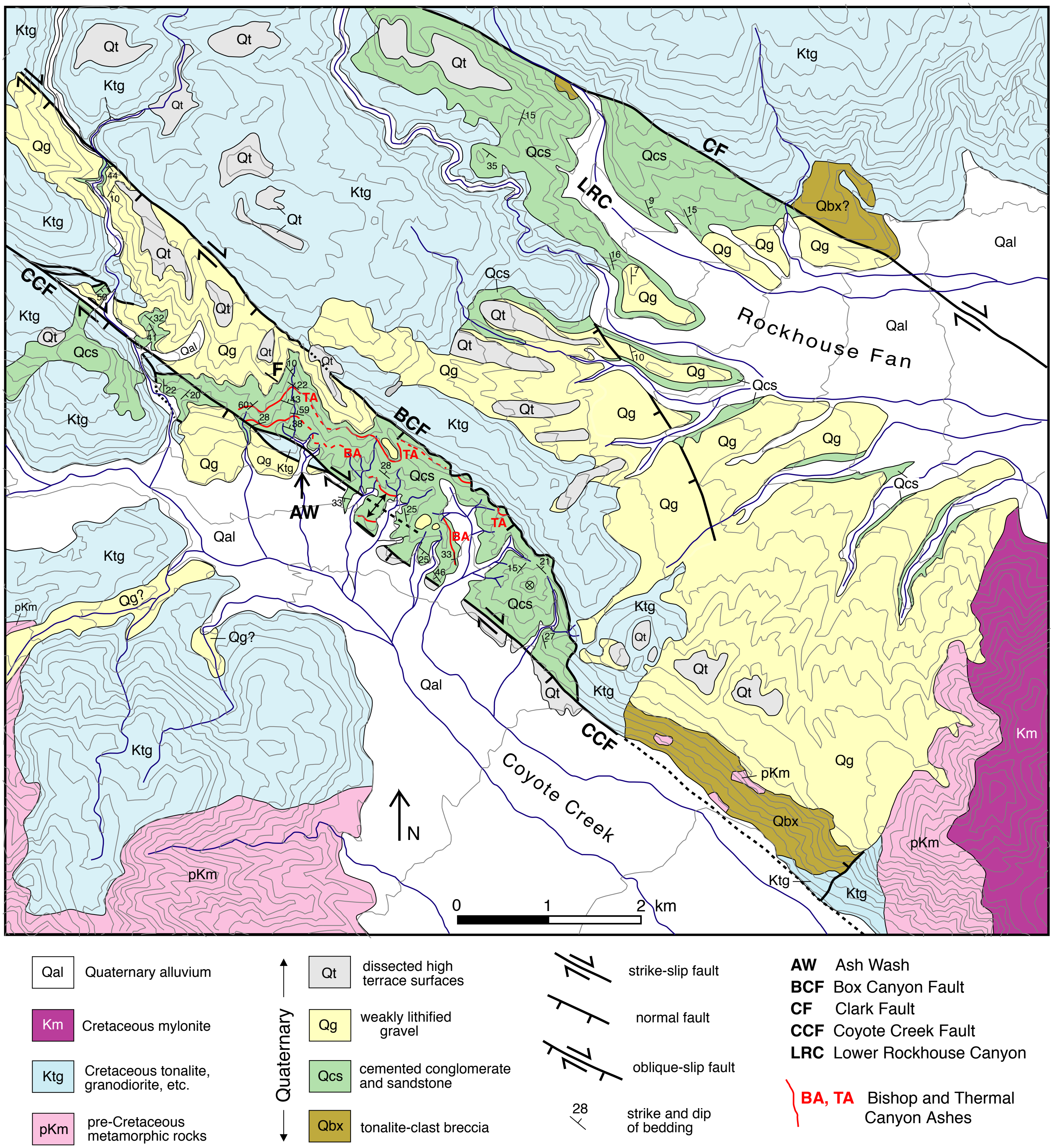

Figure 3. Geologic map of the lower Coyote Creek area. Coyote Badlands is the area of eroding Qcs (sedimentary rocks) and Qg (gravel) bounded by the Box Canyon and Coyote Creek faults. Thin gray lines are topographic contours, contour interval 40 meters. Line "F" shows position and orientation of fulcrum of tilting (neutral line) as determined for fanning-dip growth structure in Figure 9. Most contacts within crystalline rocks (pKm, Ktg, Km) are from Sharp (1967).

vertical slip rate of ~1.0 mm/yr (dePolo and Anderson, 2000). Despite these well-developed large-scale features, modern fan channels do not show observable offset on the Santa Rosa fault, and late Pleistocene alluvial fans in the hanging wall (southwest side) of the fault are currently being bypassed and eroded. These observations suggest that the Santa Rosa fault recently has become inactive and that slip ended sometime in late Pleistocene time. The Santa Rosa fault loses its expression in a zone of hummocky topography west of Rabbit Peak, and reappears as a well-defined fault scarp with triangular facets on the northeast margin of Rockhouse Valley (Fig. 2). The discontinuous aspect of the fault is not well understood; it may strike north and then cut west in the area of Rabbit Peak, or it may continue on a northwesterly trend and be buried beneath a large mass of footwall-derived landslide material.

Offset on the Clark and Coyote Creek faults is constrained by the presence of laterally continuous, moderately to steeply dipping Cretaceous mylonite in the bedrock (Fig. 2; Sharp, 1967). Sharp (1967) measured 15 km of dextral offset on the Clark fault across Clark Valley, and 5 km on the Coyote Creek fault across Borrego Valley. Remeasurement of these offsets using Sharp's map yields general agreement with minor revision: About 15 km on the Clark fault and 6 km on the Coyote Creek fault, for a total of ~21 km on the two faults. Between Anza and Hemet (Fig. 1), offset of the Thomas Mountain sill on the San Jacinto and Thomas Mountain faults is ~22–24 km (Sharp, 1967). Other studies have proposed greater amounts of total offset on the San Jacinto fault zone, ranging up to ~29–30 km (Bartholomew, 1970; Hill, 1984; Revenaugh, 1998). Measurements of offset across Borrego and Clark Valleys is considered here to be reliable because the mylonite zone is a continuous bedrock unit that provides a good strain marker. Thus, there appears to be a discrepancy between total offset measured in the study area (~21 km) versus the Anza area (~22–24 km) and farther north. This may be due to a displacement gradient on the San Jacinto fault in which slip decreases to the southeast, or distributed shear on small faults that transfer slip outside of the shear zone from northwest to southeast. West-side-down normal displacement on the Santa Rosa and Coyote Creek faults would have the effect of decreasing the amount of strike-slip offset and increasing the mismatch in offset between the different parts of the fault zone.

Restoration of offset on the Clark fault results in alignment of the Santa Rosa fault with a north-northeast-striking inactive normal fault on the west side of Coyote Mountain (Fig. 2). Mapping of crystalline rocks across the fault (Fig. 3) indicates less than ~300 m of normal offset. Correlation of this fault with the Santa Rosa fault suggests that they may once have been a single normal fault prior to offset on the Clark fault, and that slip on the older fault was terminated by initiation of the Clark fault. However, the age of this fault and its relation to older stratigraphy in this area are not well understood. Two other, old faults of uncertain age are located on the east side of Coyote Mountain and east side of the San Ysidro Mountains (west side of Borrego Valley) (Fig. 2). The east Coyote Mountain fault was inferred on the basis of gravity data by Sharp (1967), and was interpreted by Bartholomew (1970) to be an oblique-slip fault that linked the Clark and southern Coyote Creek faults during middle to late Pleistocene slip. This interpretation seems unlikely because the geomorphology on the east side of Coyote Mountain is irregular and subdued, and does not display any features diagnostic of recent fault slip, such as are seen on the Santa Rosa fault. Instead, the morphology on the east side of Coyote Mountain is similar to that of the east side of the San Ysidro Mountains; both faults display an irregular and embayed mountain range front, which suggests that the two faults are correlative and predate slip on the Coyote Creek fault. This interpretation is supported by the presence of large negative gravity anomalies in Borrego and Clark Valleys that have similar magnitude (−75 to −80 Mgal) and are oriented parallel to the inactive north-trending range fronts (Fig. 2; Bartholomew, 1970).

The Coyote Creek, Clark, and Box Canyon faults cut all Pleistocene units in the study area (Fig. 3), and therefore have a history of late Pleistocene to Holocene slip. In contrast, the normal fault on the west side of Coyote Mountain cuts older breccia (Qbx) but is overlapped by Qg gravel, indicating that this fault is older than the others. Kinematic data from the Box Canyon fault reveal slip directions clustered into strike-slip (right lateral) and dip-slip (normal) motion (Fig. 4). This reflects a complex history of movement that includes both horizontal and vertical displacement. Although it is not possible to determine the relative ages of striations in the fault zone, the stratigraphic history described below suggests that the fault initially experienced dip-slip motion during growth of a fanning-dip section in Ash Wash, and later was dominated by strike-slip motion associated with horizontal displacement on the Coyote Creek fault.

PLEISTOCENE STRATIGRAPHY OVERVIEW

Pleistocene sediments and sedimentary rocks in the study area belong to a regionally extensive sequence of sandstone, mudstone, conglomerate and breccia known informally as Bautista Beds (Frick, 1921; Sharp, 1967). These deposits are preserved in patches throughout the San Jacinto fault zone and are especially abundant and well exposed in the study area (Fig. 3). The Coyote Badlands is an area of deep canyons and vigorous erosion located between the Coyote Creek and Box Canyon faults, which provides exceptional exposures of fault-bounded Bautista beds stratigraphy (Fig. 5A). The stratigraphy is subdivided into four units (from oldest to youngest): (1) tonalite-clast breccia (Qbx; Fig. 5B), (2) bedded conglomerate and sandstone (Qcs; Fig. 5C), (3) weakly consolidated gravel (Qg; Fig. 5D), and (4) late Quaternary terrace gravels (Qt) and Holocene alluvium (Qal). This study focuses on the deposition and deformation of units 2 and 3.

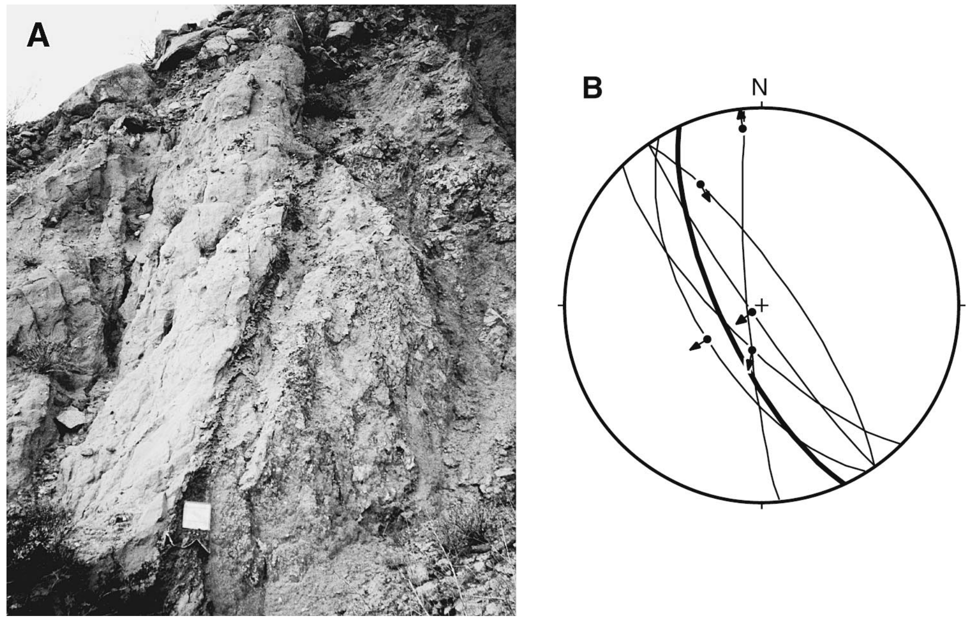

Figure 4. A: Exposure of Box Canyon fault in the Coyote Badlands near center of Figure 3, view looking northwest. Map board is 30 cm long and sits in master fault zone with well-developed clay gouge. Pleistocene sandstone and conglomerate are on left (southwest) side of fault, and brecciated Cretaceous granodiorite is on right (northeast). Fault is capped by colluvium. B: Equal area projection of fault-kinematic data from locality shown in A. Thick line is the master fault zone; thin lines are microfault planes within the fault zone and adjacent brecciated footwall. Dots with small arrows show fault striations and direction of movement of hanging wall block for each microfault. Note large variation in orientation of fault lineations, which vary from dip-slip (normal) to strike-slip (right lateral). Plot produced using Fault-Kin program by R. Allmendinger.

Tonalite-clast breccia is exposed northwest of Coyote Mountain and in a small area in lower Rockhouse Canyon (Fig. 3). At Rockhouse Canyon, Qcs depositionally overlies Qbx along a sharp uneven contact that probably is either an unconformity or the irregular upper surface of a rock avalanche deposit (Fig. 5B). This implies that Qbx is older than Qcs northwest of Coyote Mountain, and that an unconformity separates Qbx and Qg at that location. Bedded conglomerate and sandstone (Qcs) are cemented with calcite in the Coyote Badlands but are only weakly lithified in the area around lower Rockhouse Canyon. This probably reflects a difference in diagenetic history between the two areas, with deeper burial and more subsurface fluid flow inferred for well-lithified sedimentary rocks in the Coyote Badlands. The Qcs unit shows a systematic lateral facies change in the Coyote Badlands, from dominantly conglomerate in southeast to dominantly sandstone in the northwest, consistent with northwest-directed paleocurrents measured in the older part of that unit (data presented in following sections).

The Qg gravel unit is widespread in the study area. It occupies a large northeast-dipping surface northwest of Coyote Mountain, where it is located ~200 m above Coyote Creek on the northeast side of the Coyote Creek fault (Fig. 3). In this area Qg contains abundant plutonic and metamorphic clasts, with no mylonite, and imbricated clasts record transport to the northeast. It therefore is interpreted to be a beheaded gravel deposit that was derived from nonmylonitic rocks in the northern San Ysidro Mountains, on the southwest side of the Coyote Creek fault (Figs. 2, 3). It was later displaced to the southeast away from its source by strike-slip offset and at least 100–150 m of uplift due to the dip-slip component of oblique slip on the Coyote Creek fault.

ASH WASH STRATIGRAPHIC SECTION

A thick section of Pleistocene strata unconformably overlies Cretaceous plutonic rocks and is well exposed in Ash Wash in the Coyote Badlands (Figs. 3, 6). The section is 400 m thick and displays a systematic up-section increase in grain size from sandstone and pebbly sandstone (Qcs) to interbedded conglomerate and sandstone (also Qcs) to weakly lithified gravel (Qg) at the top. No tonalite-clast breccia is exposed in this section or anywhere in the structural block bounded by the Box Canyon and Coyote Creek faults. The Ash Wash section was measured at a vertical scale of ~1:200, and data were collected for sedimentary lithofacies (grain size, bed thickness, sorting, sedimentary structures, etc.), ash stratigraphy, paleocurrents, synsedimentary growth structures, and samples for paleomagnetic analyses.

Sedimentary lithofacies and depositional environments

Sedimentary rocks exposed in Ash Wash are representative of most lithologic variations (excluding tonalite breccia) observed in Pleistocene deposits in the study area. The Qcs unit (conglomerate and sandstone) makes up the lower 310 m of the measured section (Fig. 6) and consists of three main lithofacies associations: (1) sandstone and pebbly sandstone (2) conglomerate and sandstone, and (3) fine-grained sandstone with minor mudstone and claystone. The Qg unit (gravel) occupies the upper 90 m of the section. The transition from well-cemented sedimentary rocks to weakly consolidated gravel occurs in the upper ~50 m of Qcs in the transition to Qg. In the following section, lithofacies of Qcs and Qg are described and interpreted in terms of their dominant depositional processes and paleoenvironments.

Sandstone and pebbly sandstone. The lower part of the Ash Wash section is dominated by weakly bedded, poorly sorted, arkosic fine- to coarse-grained sandstone and pebbly (grussic) sandstone. These deposits contain interbedded and discontinuous thin lenses, stringers, and beds of granule to small pebble conglomerate. They are massive and structureless or display weak low-angle trough cross-bedding and planar stratification. Rare beds of siltstone and nodular calcitic sandstone are also present, some with slight admixtures of reworked ash, typically ranging up to ~50 cm thick. Some parts of the section contain 5- to 10-meter thick intervals that display weak fining-upward from thin conglomerate to sandstone and pebbly sandstone to fine-grained sandstone or siltstone (e.g., 65–80 m; Fig. 6).

Sandstone and pebbly sandstone are interpreted as the record of deposition in a sand-rich braided stream system (e.g., Walker and Cant, 1984; Miall, 1996). Trough cross-bedding was produced by deposition from sandy bars in active stream channels, and fining-up intervals resulted from lateral channel migration and abandonment. Nodular calcitic beds represent weakly developed paleosols that formed in short-lived overbank subenvironments (e.g., Retallack, 1990). The relative paucity of silt and clay rules out a meandering stream model for these facies.

Conglomerate and sandstone. This facies association displays large variations in relative abundance of conglomerate, varying from rare interbeds of conglomerate in sandstone to amalgamated thick beds of conglomerate in intervals >10 m thick (Fig. 6). Conglomerate beds are moderately sorted, clast-supported, and contain mainly pebble to cobble size clasts in a pebbly sandstone matrix. Low- to moderate-angle trough cross-bedding, lenticular discontinuous bedding, clast imbrications, and basal scour-and-fill geometries are common in pebble-cobble conglomerate where it is interbedded with sandstone (Fig. 5C). Where sandstone is present it tends to form the upper parts of fining-up intervals (e.g., 210–250 m; Fig. 6). Some beds include small boulder-size clasts (~25–40 cm diameter), with the maximum clast size ranging up to ~70 cm in the coarsest deposits. Boulder-bearing beds are internally structureless, channelized at their base, and clast-supported. Clast compositions include tonalite, granodiorite, biotite schist, quartzite, and gneiss (in roughly subequal amounts), with lesser amounts of mafic plutonic rocks.

The conglomerate and sandstone facies records deposition in a gravelly braided stream system. A fluvial origin is indicated by the presence of trough cross-bedding, which records deposition by migrating gravelly bedforms, and by weakly developed fining-up intervals (e.g., Miall, 1996). Boulder-bearing beds represent channel fill deposits that formed during large floods. An alluvial fan environment (narrowly defined; cf. Blair and McPherson, 1994) is ruled out due to the abundance of fluvial features and the lack of evidence for deposition by debris flows, sheet floods or rock avalanches. Clast compositions reflect derivation from Cretaceous plutonic rocks and pre-Cretaceous metamorphic rocks in the surrounding areas, and notably lack mylonite.

Fine-grained sandstone, mudstone, claystone. This facies association is found only between ~140 and 180 m in the section (Fig. 6), and comprises two interbedded facies. The first consists of well-sorted fine to very fine-grained sandstone and minor siltstone with abundant planar low-angle cross-bedding. Internal stratification is often difficult to see due to uniform grain size and weathering, but very fresh exposures show that it is abundant. Detrital biotite is common. One interval of sandstone contains well-developed high-angle cross-bedding in 1-m-thick bed sets. The second facies is massive, pale green to reddish claystone and mudstone seen in two 2- to 3-m-thick intervals between 150 and 180 m in the section (Fig. 6).

Fine-grained sandstone is interpreted as the deposits of eolian sand dunes. Claystone records suspension settling in standing water, probably in a small lake, fluvial floodplain, or mudflat. The close association of claystone and fine-grained sandstone implies a sediment-starved depocenter that was isolated for a short time from the input of coarse-grained sediment, allowing eolian sand dunes to form around the margins of a shallow pluvial lake or river floodplain. The tectonic significance of fine-grained sediments in this part of the section is discussed below.

Boulder-bearing gravel (Qg). Qg is a thick unit of weakly consolidated pebble-cobble to boulder-grade gravel that typically forms rubbly covered slopes in the study area, but fresh exposures in upper Ash Wash permit direct observation of the sedimentologic character of this unit. It typically contains few or no sandstone interbeds, and is characterized by broadly lenticular beds of pebble-cobble gravel that alternate with cobble-boulder beds (Fig. 5D). The deposits are moderately to poorly sorted and clast-supported, with common clast imbrication. Bedding contacts tend to be diffuse and irregular, but sharp and channelized basal contacts are also observed. Boulder-bearing beds are typically 0.5–1.5 m thick, and some show weak inverse grading and/or large boulders protruding above the top of the bed. The maximum measured clast size is ~1.5 m (long axis). Matrix-supported texture is present but rare.

Inversely graded boulder-bearing gravel beds are interpreted as the deposits of debris flows that formed on a large alluvial fan, similar to the modern Rockhouse fan in the northwest corner of Clark Valley (Fig. 3). Finer-grained, pebble-cobble conglomerate beds may also record debris-flow deposition, or they may have formed by traction transport during large flood flows.

Ash stratigraphy and paleomagnetism

The Bishop Ash is well dated at 760 ka (Sarna-Wojcicki et al., 2000), and is interbedded with sedimentary rocks at three localities in the San Jacinto fault zone: North of Anza (Sharp,

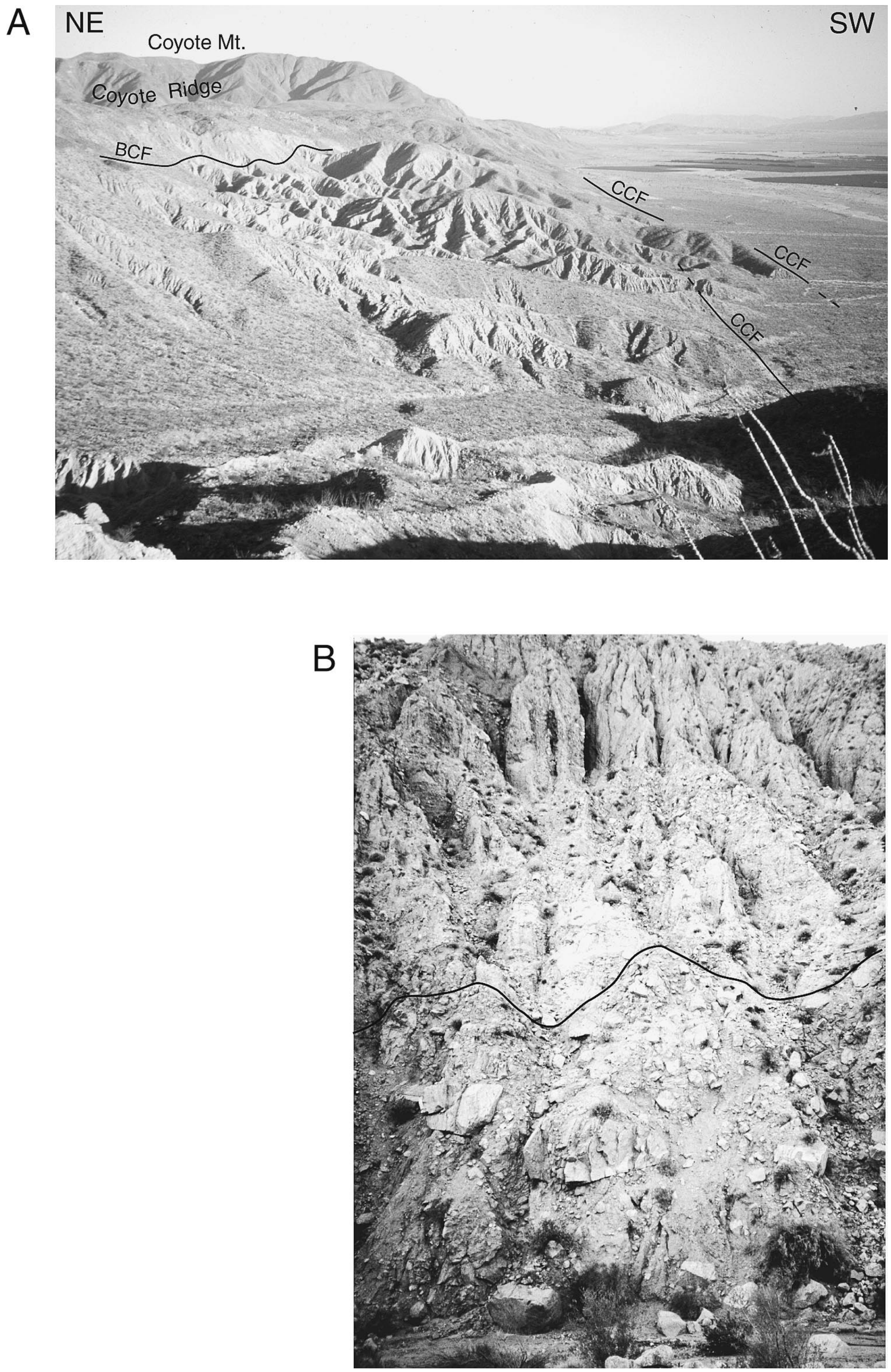

Figure 5. A: View looking southeast at deeply eroded Pleistocene deposits (mainly Qcs) in the Coyote Badlands. Box Canyon fault (BCF) on the northeast and Coyote Creek fault (CCF; two strands shown) on the southwest. Area in foreground is Ash Wash. B: Tonalite-clast breccia (Qbx) and overlying conglomerate and sandstone (Qcs) in lower Rockhouse Canyon. Irregular depositional contact (solid line) is a possible unconformity. Large block in lower middle is ~4 m long (horizontal axis). (*Continued on facing page*.)

1981), the Borrego Badlands southeast of the study area (Remeika and Beske-Diehl, 1996), and Ash Wash in the Coyote Badlands (this study; Sarna-Wojcicki et al., 1980). In Ash Wash the Bishop Ash is 1.6 m thick and consists of a 35-cm basal air-fall deposit overlain by stratified and reworked ash that is mixed with minor amounts of detrital arkosic sand and biotite. The 100 m of section above the Bishop Ash contains a series of thinner ashes, including two ash beds located 25 and 80 m above the Bishop Ash that are possible equivalents of the 740 ka ash of Thermal Canyon (Fig. 6). The Thermal Canyon ash

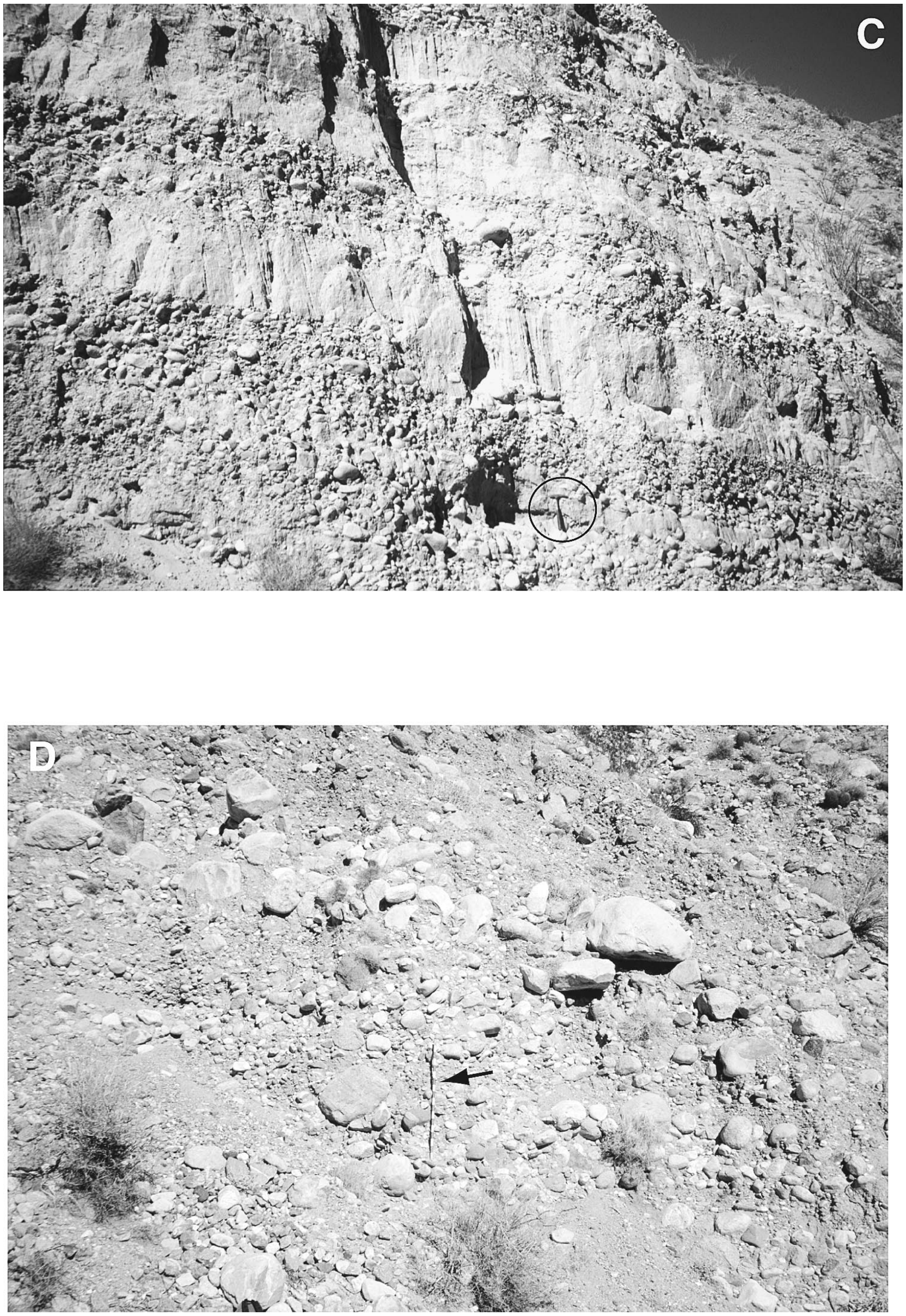

Figure 5. C: Example of interbedded conglomerate and sandstone in upper part of Qcs, Ash Wash. Hammer (circled) is 32.5 cm long. D: Example of Qg gravel exposed in upper Ash Wash. Measuring staff (indicated by arrow, near center) is 1.8 m long.

is recognized in the Mecca Hills where it occurs 40 m above the Bishop Ash, and in the Borrego Badlands 15 km southeast of the Coyote Badlands (Fig. 2) (Sarna-Wojcicki et al., 1997). The bed 80 m above the Bishop ash is a composite 1.4-m-thick ash unit with a very white (relatively pure) 50-cm-thick upper subunit that is easily traced for up to 3 km along strike to the northwest and southeast from Ash Wash. It was collected for geochemical analysis but was found to lack isotropic glass, making it unsuitable for trace element geochemistry (A. Sarna-Wojcicki, 2001, personal commun.). However, because of its relatively pure and laterally persistent character, unlike all other ashes in the section except the Bishop Ash, this unit is assigned to the Thermal Canyon Ash with a high degree of confidence.

The results of a reconnaissance paleomagnetic study in Ash Wash show that six stations collected at or above the Bishop Ash have normal polarity, and two stations located 28 and 36 m

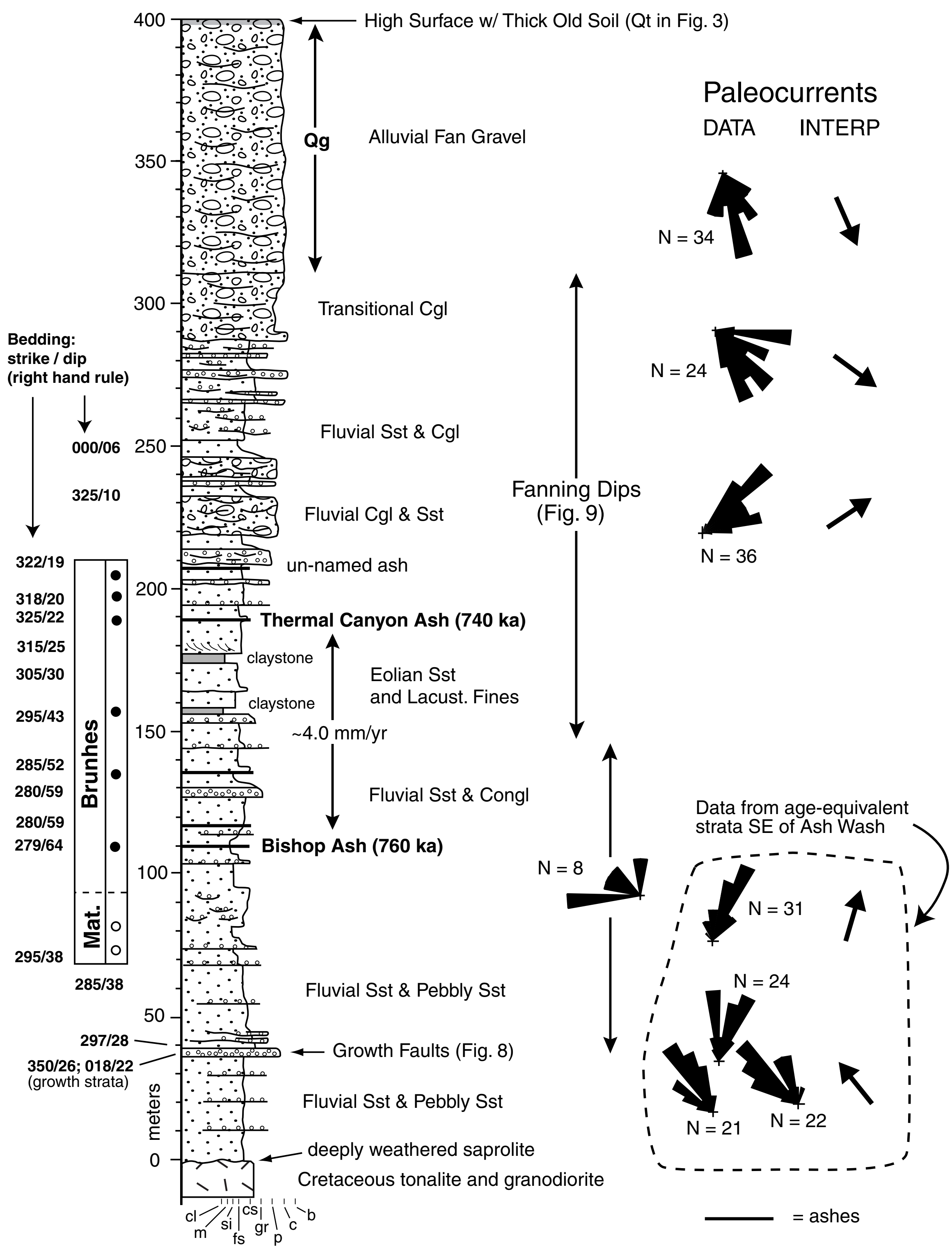

Figure 6. Measured section in Ash Wash. Dots show position of paleomagnetic samples; open circles are reversed polarity and filled circles are normal polarity. Cgl—conglomerate, sst—sandstone. Grain-size scale: cl—clay, m—mud, si—silt, fs—fine sand, cs—coarse sand, gr—granule, p—pebble, c—cobble, b—boulder. See Figure 3 for location, and text for discussion.

below the ash have reversed polarity (Fig. 6; J. Stimack, 1999, personal commun.). This is consistent with the known position of the Bishop Ash in the paleomagnetic time scale, and indicates that the Matayama-Bruhnes boundary (780 ka) is <28 m below the Bishop Ash. More detailed sampling would be needed to accurately place this polarity reversal in the section.

Sedimentation rates are constrained by stratigraphic thicknesses and ages of the magnetic polarity reversal and two ashes (Fig. 6). The Matuyama-Brunhes reversal (780 ka) is <28 m below the Bishop Ash (760 ka), giving a maximum sedimentation rate of 1.4 mm/yr in this part of the section. The actual rate is probably less than this, and is uncertain due to large sample spacing. Assuming ~0.5–1.0 mm/yr sedimentation rate for the lower part of the section in Ash Wash, the base of the section is inferred to be ca. 0.9–1.0 Ma. The Thermal Canyon ash is 80 m above the Bishop ash, which records an increase in sedimentation rate to ~4 mm/yr. This rate is rapid but not unreasonable for an area of active fault controls on subsidence and sedimentation.

Age of Qg gravel

In most places the basal contact of Qg is an angular unconformity where it overlies older dipping Pleistocene sediments (Qbx and Qcs), or it is a nonconformity where it rests on crystalline basement rocks. One important exception to this is found in Ash Wash (Fig. 3) where Qg conformably overlies Qcs sandstone and conglomerate in the down-tilted part of a Pleistocene growth structure (described below). The age of Qg is not known from direct dating, but it can be inferred using the age of older deposits and the stratigraphic thickness from dated older deposits to the top of Qg. The conformable base of Qg is 120 m above the 740 ka Thermal Canyon Ash (Fig. 6), and its thickness ranges up to ~120–140 m in areas northwest and southeast of Ash Wash (Fig. 3). This gives a total thickness of ~250 m from the Thermal Canyon Ash to the top of Qg. Assuming a range of likely sedimentation rates (1–4 mm/yr), the possible duration of time represented by this thickness is ~60–250 k.y. The top of Qg is thus bracketed between 490 and 680 ka (rounded to ca. 600 ± 100 ka). Although Pleistocene climate variations are not well known in this area, it is likely that bracketing the sedimentation rate between 1 and 4 mm/yr encompasses the variations that might have occurred due to variations in rainfall and erosion rate.

Paleocurrents

Paleocurrent data were collected from Qcs and Qg units in the Coyote Badlands and lower Rockhouse Canyon (Figs. 6, 7). The data were obtained from imbricated clasts, cross-bedding, current lineations, and channel axes, with the majority of measurements obtained from clast imbrications. Paleocurrents in Ash Wash and elsewhere in the Coyote Badlands (Fig. 6) show a systematic reversal through the section, from north-

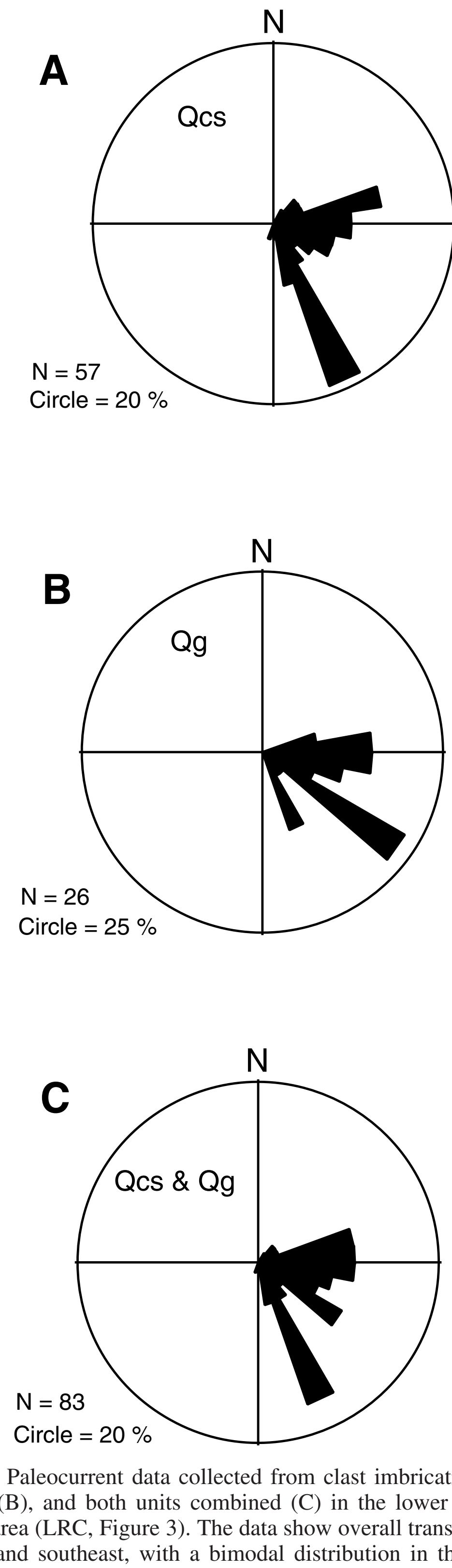

Figure 7. Paleocurrent data collected from clast imbrications in Qcs (A), Qg (B), and both units combined (C) in the lower Rockhouse Canyon area (LRC, Figure 3). The data show overall transport toward the east and southeast, with a bimodal distribution in the Qcs-only data. Paleocurrents record sediment dispersal to the southeast along the Clark fault valley, and to the east-northeast due to a component of northeastward tilting toward the Clark fault.

west-directed in lower Qcs to northeast- and then southeast-directed in upper Qcs and Qg. This change begins gradually below the Bishop Ash, and the main change occurs across the interval of fine-grained eolian and lacustrine deposits between 150 and 180 m (Fig 6). Northwest-directed paleocurrents in the lower part of the section are opposed to the overall direction of stream flow in modern Coyote Creek and its tributaries, but they are consistent with observed lateral fining of facies in lower Qcs from mainly conglomerate in the southeast to mainly sandstone in the northwest. In contrast to the Coyote Badlands, lower Qcs deposits in and around lower Rockhouse Canyon near the Clark fault show transport dominantly to the east and southeast, consistent with modern drainages in that area (Figs. 3, 7). This indicates that the Clark fault was active and formed a fault valley during deposition of Qcs, and continued to influence drainage patterns during Qg deposition. A prominent component of transport toward the east-northeast in Qcs (Fig. 7A) probably is due to northeastward tilting toward the Clark fault during this time.

Growth structures

Two sets of growth structures with different orientations are exposed in Ash Wash: (1) small northeast-striking normal faults low in the section (Fig. 8), and (2) a large northwest-striking fanning-dip section and progressive unconformity higher in the section (Figs. 6, 9).

In the lower part of the section, several growth faults strike northeast, dip northwest, and cut sedimentary units that show pronounced thickness changes and up-section decrease in offset across the faults (Fig. 8). The strike of bedding is slightly different than that of the faults, suggesting a component of strike-slip displacement, but the displacement geometries indicate that the faults record dominantly small-scale dip-slip (normal) offset. These faults are overlapped by probable late Pleistocene terrace gravel deposits set into the modern Ash Wash. Farther up section a normal fault with the same orientation cuts the Bishop Ash, lacks brittle fault features, and is filled with a sand dike injected by liquefaction from the lower part of the faulted ash deposit. These features record extensional or transtensional deformation on northeast striking, northwest dipping faults during deposition of the lower part of Qcs in Ash Wash. This orientation is similar to the northeast-striking normal fault that cuts Qbx breccia on the northwest side of Coyote Mountain (Figs. 2, 3), and they are interpreted to be genetically related.

The second growth structure occupies the upper part of the Ash Wash section (Figs. 6, 9). Figure 9 shows a systematic up-section decrease in bedding dips, from 43° in the lower part through 20° to subhorizontal in Qg (Fig. 9). The fanning-dip interval is capped by a progressive unconformity in which the contact itself changes laterally from a well-defined angular unconformity on the left (southwest) to a completely conformable contact on the right (northeast) (Fig. 9). The lateral change from unconformity to conformable contact takes place through a zone of complex lateral interfingering and onlapping. The fanning dips and progressive unconformity preserve a record of northeastward tilting, erosion, and sedimentation during deposition of upper Qcs and transition to Qg gravel. The fulcrum of tilting (neutral line) is located about half way between the Coyote Creek and Box Canyon faults (Fig. 3), and it is inferred that slip on these faults controlled syn-depositional tilting.

Because strike-slip offset on the Qg unit is equal to total

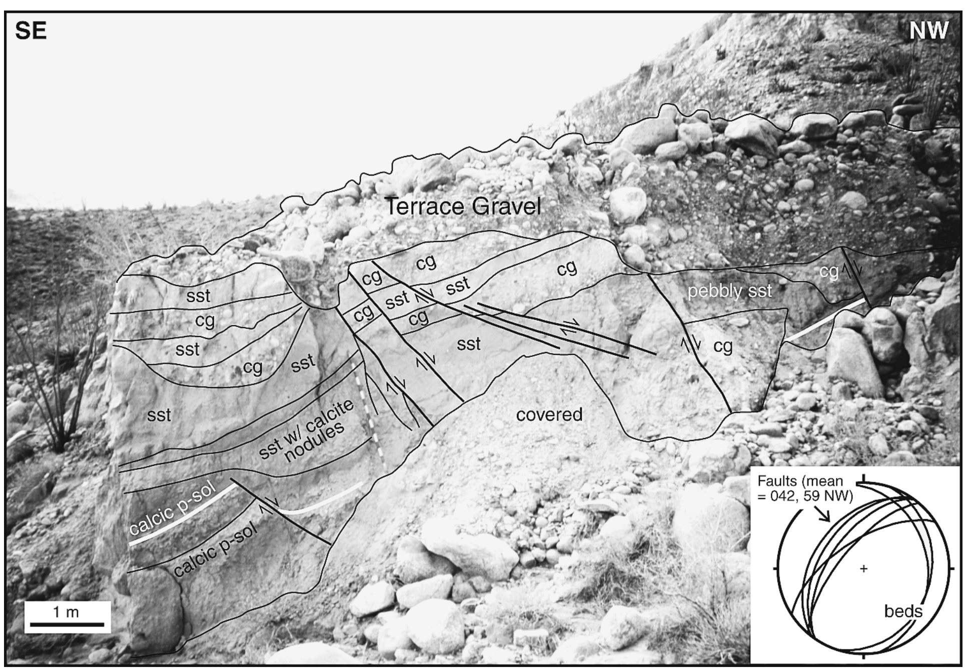

Figure 8. Close-up view of growth faults exposed in the lower part of Ash Wash section (Fig. 6), view looking southeast. Bold white line represents correlatable, offset calcic paleosol (p-sol) horizon. Note upward decrease in slip and draping of strata over fault on left side. Inset shows equal-area stereonet projection of faults and bedding planes in this exposure.

displacement on the Coyote Creek fault (Figs. 2, 10), the phase of tilting represented by fanning dips must predate the onset of strike-slip offset. This, combined with the lack of similarly oriented growth structures lower in the section and the position of the fulcrum of tilting, all support the interpretation that the fanning-dip structure records the earliest, initial phase of slip on the Coyote Creek and Box Canyon faults in the Coyote Badlands at 750 ka (Fig. 6). The derived sense of offset is dip-slip (normal), down on the southwest side of the bounding faults, with no evidence for strike-slip displacement during the initial phase of fault slip. A vertical component of displacement and northeastward tilting is further indicated for the Box Canyon fault by juxtaposition of thick sedimentary rocks southwest of the fault directly against Cretaceous plutonic rocks on the northeast side, progressive increase in thickness of Qcs to the northeast away from the fault (Fig. 3), and down-dip lineations in the fault zone (Fig. 4). Evidence for dip-slip offset on the Coyote Creek fault is seen in the large fault sliver of Cretaceous plutonic rock in lower Ash Wash, and the fact that the large area of stranded Qg gravel on the northeast side of the Coyote Creek fault sits ~120 m above the present elevation of its source valleys on the southwest side of the fault (Fig. 3).

INTERPRETATION OF VERTICAL TRENDS

The above information provides insights into the evolution of depositional environments, sediment-dispersal patterns, subsidence rates, and surface deformation during Pleistocene faulting and sedimentation. Deposition of Qbx may have resulted from movement on the Santa Rosa and west Coyote Mountain faults, prior to displacement on the Clark fault, but the timing and controls on this early phase of sedimentation are not well understood. The lower part of Qcs in lower Rockhouse Canyon was deposited in a southeast-flowing valley, providing evidence that the Clark fault was initiated sometime prior to Qcs deposition. The up-section reversal of paleocurrents in Ash Wash, from northwest- to southeast-directed, can be understood in the context of regional structural controls on geomorphology and stream evolution in the San Jacinto fault zone. Initiation of the Clark fault at ca. 1.5 Ma is believed to have breached the former Peninsular Ranges divide and created steep new drainages that flowed southeast to the Salton Sea, causing reorganization of the regional stream system and widespread drainage reversals that are still active today (Dorsey and Ryter, 2000; Dorsey, 2001). The reversal in paleocurrents at Ash Wash is believed to be part of these regional stream captures, and is related to the complex evolution of drainages as controlled by slip on the Clark and Coyote Creek faults (see below).

Figure 6 shows that very rapid sedimentation (~4 mm/yr) coincided with a reversal in paleocurrent directions, onset of northeastward tilting, and deposition of the finest-grained sediments in the section. The synchronous occurrence of these changes suggests that they are genetically related, and are interpreted to record initiation of dip-slip movement on the Coy-

Figure 9. Photomosaic with interpretation of fanning-dip section and progressive unconformity in upper Ash Wash. This growth structure records initiation of the Coyote Creek and Box Canyon faults by dip-slip (normal) displacement and syndepositional tilting to the northeast. Congl—conglomerate, sst—sandstone. See Figure 3 for location and Figure 6 for stratigraphic position.

ote Creek and Box Canyon faults. Rapid production of accommodation space by fault slip temporarily trapped coarse detritus in a small area of subsidence close to the Box Canyon fault, causing development of a small lake basin with limited input of fine-grained eolian sand and silt. Northwest-flowing streams that formerly were connected to a larger, west flowing regional stream system were captured by streams flowing southeast along the Clark fault, probably due to this faulting episode. A new source area located to the northwest along the present-day Coyote Creek supplied a large volume of coarse gravel, possibly reworked from older deposits, which quickly filled the small lacustrine depocenter with a prograding boulder-rich alluvial fan. This situation probably resembled the modern advance of the bouldery Rockhouse fan into the northwest corner of Clark Valley (Fig. 3).

COYOTE CREEK FAULT RECONSTRUCTION

Restoration of strike-slip offset

In order to interpret the history of fault slip, it is useful to restore total strike-slip offset on the Coyote Creek fault. The reconstruction is produced by correlating the western contact of mylonite across the Coyote Creek fault, from Coyote Mountain on the northeast side to the eastern San Ysidro Mountains on the southwest (Figs. 2, 3, 10). The age of this reconstruction coincides with the end of Qg deposition, which is uncertain but is bracketed between ca. 500 and 700 ka (see above). There is some uncertainty in the amount of strike-slip offset because the mylonite contact with plutonic and metamorphic rocks is not exposed immediately adjacent to the Coyote Creek fault on the southwest side of the fault, and therefore is projected northward beneath alluvium in northern Borrego Valley (Figs. 2, 10). The mylonite contact trends approximately due north at Coyote Mountain and ~020° in the eastern San Ysidro Mountains, and it probably does not vary significantly from this trend where it is covered. Accounting for these uncertainties, ~6 km of right lateral offset is measured on the Coyote Creek fault. It is difficult to quantify the uncertainty in this measurement, but the error is probably ~0.5–1 km.

Because the mylonite dips to the east, any southwest-side-down offset on the Coyote Creek fault due to northeastward tilting would produce a component of apparent right-lateral separation that is not due to strike-slip offset. The importance of

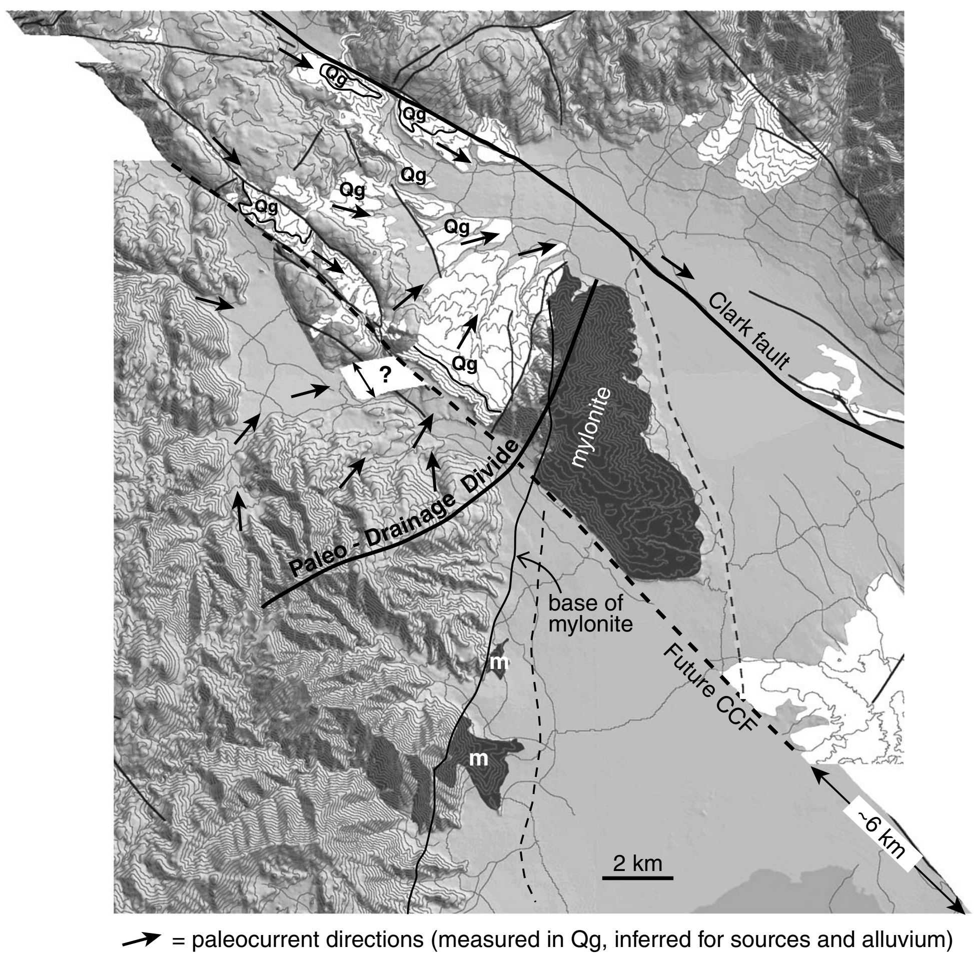

Figure 10. Reconstruction of Coyote Creek fault (CCF) during Qg deposition, prior to onset of strike-slip displacement on the fault. Restores strike-slip displacement only, and does not restore vertical fault offsets or surface erosion. Position of paleo-drainage divide is based on measured paleocurrent directions and inferred sources for Qg gravel.

this effect can be evaluated by comparing fault offset measured on the mylonite with that of displaced Quaternary deposits. Geomorphic and geologic maps, clast compositions, and paleocurrents all show that Qg gravel was derived from northeast-draining streams located in the northern San Ysidro Mountains (Figs. 2, 3, 10). Restoration of ~6 km of strike-slip offset on the Coyote Creek fault restores a wide area of Qg downstream from that source, with the southeast margin of Qg located slightly southeast of the easternmost feeder channel (Fig. 10). This pattern is consistent with downstream widening of the channel that is expected for catchments and alluvial fans. Thus, the total strike-slip offset on Qg is virtually the same as offset measured on the bedrock contact between mylonite and plutonic rocks. Although there is evidence for some dip-slip displacement of Qg on the Coyote Creek fault (~100–150 m), and probably somewhat more on older sediments and bedrock, it is not enough to produce a large artificial component of apparent strike-slip separation on the fault.

The timing and average rate of slip can be estimated from the above information. Strike-slip offset on the Coyote Creek fault began sometime after deposition of Qg. Thus, total offset of ~6.0 ± 1 km since 600 ± 100 ka gives a time-averaged slip rate of ~10 ± 3 mm/yr. The reconstruction in Figure 10 shows that, prior to strike-slip offset on the Coyote Creek fault, high topography in Coyote Mountain and the San Ysidro Mountains formed a drainage divide that controlled sediment transport. Qg gravel preserved on the gently northeast-dipping slope west of Coyote Mountain was derived from the northern San Ysidro Mountains and transported northeastward into Clark Valley. North and northwest of this slope of Qg, in the area of lower Rockhouse Canyon, paleocurrent data show that Qg sediment was transported toward the east and southeast (Figs. 7, 10) indicating that the Clark fault was active during this time.

Fault-slip and sedimentation history

Using data and explanations presented above, it is possible to reconstruct the history of sedimentation as controlled by faulting in the Coyote Badlands and surrounding areas (Fig. 11). Deposition of the oldest sediments in the Coyote Badlands (lower Qcs, pre–760 ka) took place prior to initiation of the Coyote Creek fault (Fig. 11A). Sediment derived from the northern San Ysidro Mountains was transported along two pathways: (1) northwest through what is now the Coyote Badlands, and (2) northeast into Clark Valley and then southeast along the Clark fault. The northwest-flowing streams are believed to be a remnant of a regional stream system that flowed to the west off the high Santa Rosa and San Jacinto Mountains prior to initiation of the San Jacinto fault zone (Dorsey and Ryter, 2000; Dorsey, 2001). By ca. 800 ka the former regional stream network had been partially disrupted by stream captures resulting from early slip on the Clark fault, producing the complex paleocurrent patterns shown in Figure 11A. Gravel was transported southeast along the Clark fault (Fig. 7) and into the Borrego Badlands where it is represented by the Ocotillo Formation. The Borrego Badlands may have been a subsiding pull-apart basin during this time, but the evidence for that hypothesis is inconclusive (see Discussion).

By ca. 600 ka several significant changes had occurred: (1) the Coyote Creek and Box Canyon faults were initiated by dip-slip normal offset, as recorded in the fanning dip section and progressive unconformity in Ash Wash, (2) streams in the Coyote Badlands had reversed direction and now flowed to the southeast, and (3) southeast-flowing streams in the Coyote Badlands turned and flowed northeast into Clark Valley where they joined the active Clark fault (Fig. 10, 11B).

By ca. 400 ka (Fig. 11C), early strike-slip offset on the Coyote Creek fault had breached the drainage divide that formerly connected Coyote Mountain to the San Ysidro Mountains. This created a new fault valley that flowed southeast into Borrego Valley and established the modern drainage pattern. Broad uplift and northeastward tilting of Qg on the northeast side of the fault, combined with strike-slip displacement away from its source in the San Ysidro Mountains, caused a large area of previous Qg deposition to be abandoned and eroded. Clark Valley had probably become a closed depression by this time, but the timing of that transition is not well known. Figure 11D shows the modern geomorphology and present stage of fault-zone development.

DISCUSSION

The data and reconstructions presented above provide new insights into the history of initiation and subsequent slip on the Coyote Creek fault in the lower Coyote Creek area, but the relationship of these events to evolution of the San Jacinto fault zone at the regional scale remains uncertain. This uncertainty is represented by two structural models that are mutually exclusive but appear to be equally supported and contradicted by existing data. In the first hypothesis, the southern Coyote Creek fault (southeast of the Borrego Badlands; Figs. 1, 2) is the same age as the Clark fault and was connected to the Clark fault via a normal fault on the east side of Coyote Mountain prior to ca. 600 ka (e.g., Bartholomew, 1970; Fig. 11A, B). In this model, Pleistocene sedimentary rocks exposed in the Borrego Badlands were deposited in a pull-apart basin, and initiation of the Coyote Badlands strand represents northwestward propagation of the Coyote Creek fault, transfer of slip from the Clark fault to the Coyote Creek fault, and straightening of the San Jacinto fault zone which continues today. In the second hypothesis, the whole Coyote Creek fault was initiated along most or all of its length at the same time as the Coyote Badlands strand, at ca. 600 ± 100 ka. In either case, I infer that the old normal faults on the east side of Coyote Mountain and the San Ysidro Mountains, and the associated linear gravity lows seen in the flanking modern valleys (Bartholomew, 1970), represent dissected remnants of the breakaway of a regional low-angle normal fault (detachment) system that was active in the western Salton

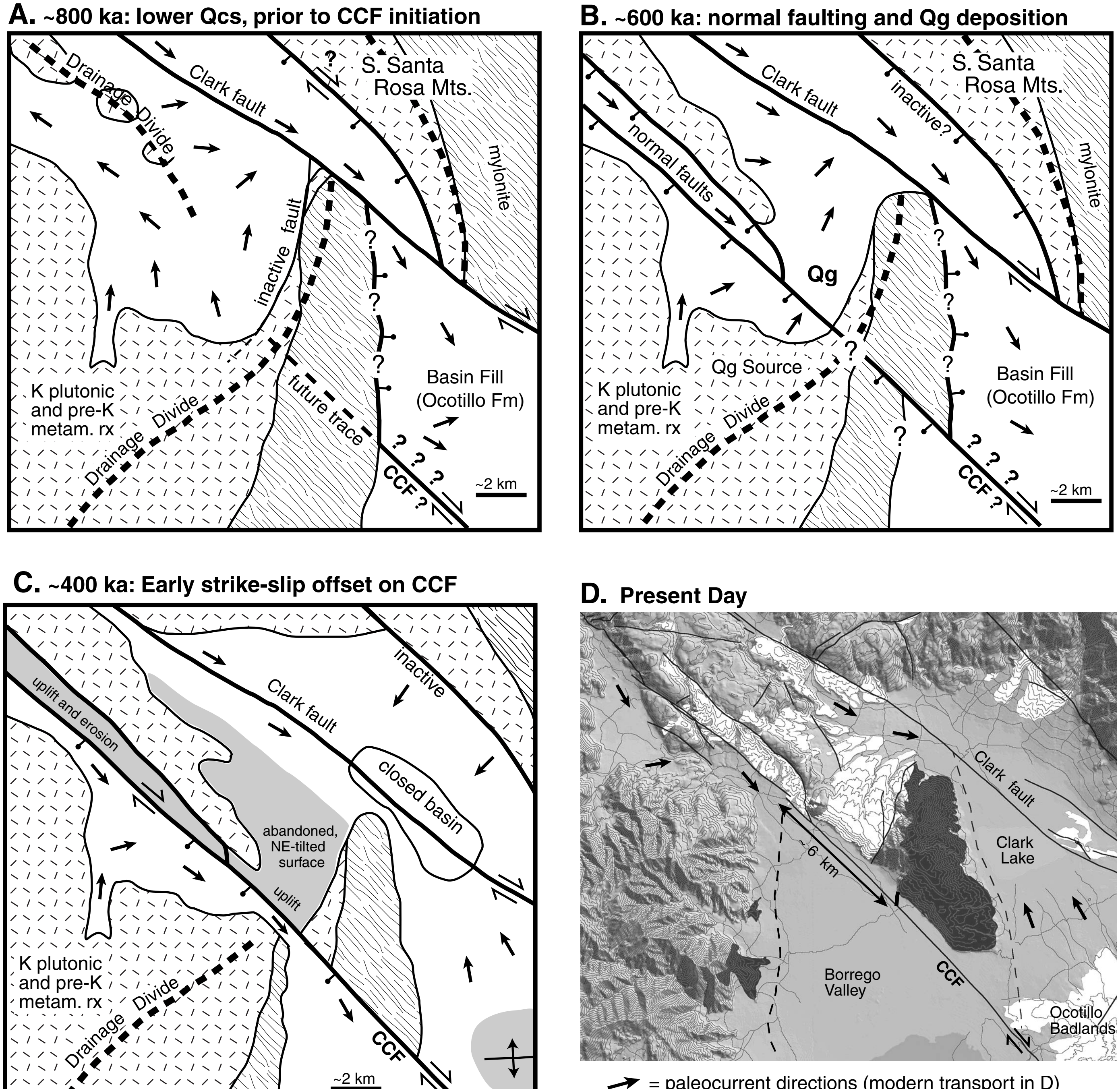

Figure 11. Four-stage reconstruction of the Coyote Creek fault (CCF) and adjacent areas since ca. 800 ka. A: Prior to initiation of the CCF (ca. 800 ka), lower Qcs sand and gravel were deposited in a complex setting that included both inherited (northwest-flowing) and young (southeast-flowing) streams. B: By 600 ka, prior to strike-slip displacement on the CCF, the Coyote Creek and Box Canyon faults had been initiated by dip-slip normal offset. Sediment transport in the Coyote Badlands had reversed, and Qg gravel accumulated in a large alluvial fan system that drained to the Clark fault valley. C: Early strike-slip offset on the CCF resulted in breaching of the former drainage divide and initiation of sediment transport to the southeast along the fault; northeastward tilting and abandonment of Qg gravel on Coyote Ridge; and onset of folding in the Ocotillo Badlands. D: Present-day setting shows active faulting controls on modern topography and streams. Paleocurrent data used to reconstruct sediment-dispersal patterns are shown in Figures 6 and 7.

Trough from late Miocene to early Pleistocene time (Axen and Fletcher, 1998). In the following section, I briefly summarize the evidence for and against these two hypotheses and discuss their regional tectonic implications.

The fault-jog (pull-apart basin) hypothesis is supported by (1) the large thickness of Pleistocene sedimentary rocks in the Borrego Badlands compared to areas southwest of the Coyote Creek fault (Dibblee, 1954, 1984), (2) the short distance over which the Clark fault dies out to the southeast into deformed Pleistocene strata (Fig. 2), and (3) the geometry of the Coyote Creek fault, which is favorably oriented to simplify and straighten the San Jacinto fault zone through time (Figs. 1, 2; cf. Wesnousky, 1988; Zhang et al., 1989). The fault-jog hypothesis is contradicted by (1) apparent lack of unconformities in the thick sedimentary section exposed in and south of the Borrego Badlands, which should form during creation of a pull-apart basin due to strike-slip faulting, (2) widespread regional distribution of the Ocotillo Formation, which should be restricted to the Borrego Badlands if it accumulated in a localized pull-apart basin, (3) subdued morphology and apparent old age of the normal fault on the east side of Coyote Mountain, and its likely correlation to the old fault on the west side of Borrego Valley (Fig. 2), (4) probable similarity of offset (~6 km) on the Coyote Creek fault northwest and southeast of the Borrego Badlands, although this is not well constrained, and (5) presence of abundant fresh fault scarps, shutter ridges, and offset stream channels along the Clark fault, suggesting that it has been at least as active as the Coyote Creek fault during late Pleistocene and Holocene time. If the fault-jog hypothesis is not correct, then the southern Coyote Creek fault does not share an older slip history with the Clark fault and instead was initiated along most or all of its length at ca. 600 ± 100 ka. It is beyond the scope of this paper to attempt a full presentation of data for and against the fault-jog hypothesis, but it appears from this summary that the question presently is unresolved.

The only widespread coarse-grained clastic unit in the western Salton Trough (Fig. 1) is the Ocotillo Formation, which ranges in age from 1.2 to ca. 0.6 Ma (Remeika and Beske-Diehl, 1996; Dibblee, 1954). The base of the Ocotillo (1.2 Ma) has recently been interpreted to represent a large pulse of sediment that prograded into the basin in response to initiation of the Clark fault and a related history of regional stream captures in the Peninsular Ranges (Dorsey and Ryter, 2000; Dorsey, 2001). The lag time between fault initiation and arrival of coarse sediment in the Borrego Badlands is difficult to determine and may plausibly range from ~100–500 k.y. Given the existing uncertainties, initiation of the Clark fault (and thus the San Jacinto fault zone) is tentatively estimated to be ca. 1.5 ± 0.2 Ma. Combining this age estimate with total slip of 22–24 km on the San Jacinto fault zone (Sharp, 1967) yields a time-averaged slip rate of ~13–18 mm/yr. This is only slightly faster than the late Pleistocene slip rate (13 mm/yr) favored by Rockwell et al. (1990) near Anza, where large uncertainties exist due to the difficulty of estimating absolute ages from soil chronology, and is consistent with an estimate of 15 ± 3 mm/yr determined from paleoseismology in the Anza area (Merifield et al., 1989).

The two hypotheses described above have different implications for the history of strike-slip faulting and basin evolution in the western Salton Trough. If the fault-jog hypothesis is correct, it implies that the southern Coyote Creek fault shares an older slip history with the Clark fault and that both were initiated ca. 1.5 Ma, or possibly earlier. In this case, initiation of the Coyote Badlands strand of the Coyote Creek fault would represent a relatively minor straightening and reorganization of the San Jacinto fault zone. Alternatively, if the Coyote Creek was initiated along most of its length at ca. 600 ka, early slip on the Clark fault may have been accommodated by growth of contractional folds and faults in the San Felipe Hills, southeast of the Borrego Badlands (Feragen, 1986; Wells, 1986). In this reconstruction, north-south shortening in the San Felipe Hills occurred in a large restraining step-over between the Clark and Imperial faults, and increasing resistance to transpressional deformation may have caused initiation of the Coyote Creek fault at ca. 600 ka (Ryter and Dorsey, 2002). In a possible hybrid of these hypotheses, pre–600 ka slip on the Clark fault may have been linked to now-inactive faults on the northeast margin of the Fish Creek and Vallecito Mountains (Dibblee, 1954) in a releasing-bend geometry that was terminated by initiation of the modern Coyote Creek, Superstition Mountain, and Superstition Hills faults. These models make a number of testable predictions about stratigraphic and structural relationships in the western Salton Trough, and highlight the need for future studies of the geologic evolution of the San Jacinto fault zone in this region.

CONCLUSIONS

The Pleistocene history of initiation and slip on the Coyote Badlands strand of the Coyote Creek fault, central San Jacinto fault zone, is recorded in thick sedimentary deposits, active faults, and geomorphology of the lower Coyote Creek area. Sedimentary units include tonalite-clast breccia (Qbx), conglomerate and sandstone (Qcs) and weakly consolidated boulder-bearing gravel (Qg). The age of the deposits is known from the presence of the Bishop Ash (760 ka) and Thermal Canyon Ash (740 ka) interbedded in the Qcs units. Qbx and Qg were deposited in alluvial fan environments, and Qcs accumulated in a sandy fluvial setting that was punctuated in the Coyote Badlands by formation of a short-lived shallow lake or mudflat with fringing eolian dunes.

The upper part of Qcs contains a large growth structure comprising a thick section of fanning dips and progressive unconformity, which records initiation of the Coyote Creek and Box Canyon faults by dip-slip (normal) displacement beginning at 750 ka. Qg gravel conformably overlies the growth structure, and its top (~250 m above the Thermal Canyon Ash) is inferred to be ca. 600 ± 100 ka. Offset of Qg is equal to the total strike-slip displacement (~6 km) on the Coyote Creek fault. Therefore, all strike-slip motion on the Coyote Creek fault in the study area has occurred since ca. 600 ka, and the time-averaged slip rate is ~10 mm/yr. The relation of these events to the regional evolution of the San Jacinto fault zone remains uncertain.

ACKNOWLEDGMENTS

Funding for this study was provided by the National Science Foundation (EAR-9805794). The author gratefully acknowledges support and collecting permits from the Anza Borrego Desert State Park of California. George Jefferson is thanked for years of logistical and moral support. John Stimack and Ray Weldon assisted with the paleomagnetic study; Derek Ryter provided minor additions to the geologic map and assisted with GIS image analysis. Discussions with Derek Ryter, George Jefferson, Susanne Janecke, Tom Rockwell, and Ray Weldon provided valuable insights and motivation during the course of this study. Steve Graham, Karen Grove, George Jefferson, and Andy Barth are thanked for constructive reviews of the manuscript.

REFERENCES CITED

Albright, L.B., III, 1999, Magnetostratigraphy and biochronology of the San Timoteo Badlands, Southern California, with implications for local Pliocene-Pleistocene tectonic and depositional patterns: Geological Society of America Bulletin, v. 111, p. 1265–1293.

Axen, G.J., and Fletcher, J.M., 1998, late Miocene–Pleistocene extensional faulting, northern Gulf of California, Mexico and Salton Trough, California: International Geology Review, v. 40, p. 217–244.

Bartholomew, M.J., 1970, San Jacinto fault zone in the northern Imperial valley, California: Geological Society of America Bulletin, v. 81, p. 3161–3166.

Bennett, R.A., Rodi, W., Reilinger, R.E., 1996, Global Positioning System constraints on fault slip rates in Southern California and northern Baja, Mexico: Journal of Geophysical Research, v. 101, p. 21 943–21 960.

Blair, T.C., and McPherson, J.G., 1994, Alluvial fans and their natural distinction from rivers based on morphology, hydraulic processes, sedimentary processes, and facies assemblages: Journal of Sedimentary Research, v. 64, p. 450–489.

DeMets, C., 1995, Reappraisal of seafloor spreading lineations in the Gulf of California: Implications for the transfer of Baja California to the Pacific plate and estimates of Pacific-North America motion: Geophysical Research Letters, v. 22, p. 3545–3548.

DeMets, C., Gordon, R.G., Argus, D.F., Stein, S., 1994, Effect of recent revisions to the geomagnetic reversal time scale on estimates of current plate motions: Geophysical Research Letters, v. 21, p. 2191–2194.

dePolo, C.M., and Anderson, J.G., 2000, Estimating the slip rates of normal faults in the Great Basin, USA: Basin Research, v. 12, p. 227–240.

Dibblee, T.W., Jr., 1954, Geology of the Imperial Valley region, California, *in* Jahns, R.H., ed., Geology of southern California: California Division of Mines Bulletin 170, p. 21–28.

Dibblee, T.W., 1984, Stratigraphy and tectonics of the San Felipe Hills, Borrego Badlands, Superstition Hills and vicinity, *in* Rigsby, C.A., ed., The Imperial Basin: Tectonics, sedimentation and thermal aspects: Los Angeles, California, Pacific Section Society of Economic Paleontologists and Mineralogists Field Trip Guidebook, v. 40, p. 31–44.

Dorsey, R.J., 2001, Two-stage evolution of the San Jacinto fault zone: Crustal response to Pleistocene oblique collision along the San Andreas fault: Eos (Transactions, American Geophysical Union), v. 82, p. F933.

Dorsey, R.J., and Ryter, D.W., 2000, Stratigraphic and geomorphic evidence for Pleistocene initiation of the San Jacinto fault zone: Eos (Transactions, American Geophysical Union), v. 81, p. 1141–1142.

Feragen, E.S., 1986, Geology of the southeastern San Felipe Hills, Imperial Valley, California [M.Sc. thesis]: San Diego, California, San Diego State University, 144 p.

Frick, C., 1921, Extinct vertebrate faunas of the Badlands of Bautista Creek and San Timoteo Canyon, southern California: California University, Department of Geology Bulletin, v. 12, p. 277–424.

Hill, R.I., 1984, Petrology and petrogenesis of batholithic rocks, San Jacinto Mountains, Southern California [Ph.D. thesis]: Pasadena, California, California Institute of Technology, 731 p.

Humphreys, E.D., and Weldon, R.J., 1994, Deformation across the western United States: A local estimate of Pacific-North America transform deformation: Journal of Geophysical Research, v. 99, p. 19 975–20 010.

Kendrick, K., McFadden, L., Morton, D., 1994, Soils and slip rates along the northern San Jacinto fault, *in* McGill, S.F., and Ross, T.M., eds., Geological investigations of an active margin: Geological Society of America, Cordilleran Section Annual Meeting Field trip Guidebook., v. 27, p. 146–151.

Matti, J.C., Morton, D.M., and Cox, B.F., 1992, The San Andreas fault system in the vicinity of the central Transverse Ranges province, Southern California: U.S. Geological Survey Open-File Report OF 92-0354.

Merifield, P.M., Rockwell, T.K., Loughman, C.C., and Klinger, R.E., 1989, Study of seismic activity by selective trenching along the San Jacinto fault zone, southern California: U.S. Geological Survey, Final Technical Report 89-1, 24 p.

Miall, A.D., 1996, The geology of fluvial deposits: Sedimentary facies, basin analysis, and petroleum geology: Berlin, New York, Springer-Verlag, 582 p.

Morton, D.M., and Matti, J.C., 1993, Extension and contraction within an evolving divergent strike-slip fault complex: The San Andreas and San Jacinto fault zones at their convergence in Southern California, *in* Powell, R.E., et al., eds., The San Andreas fault system: Displacement, palinspastic reconstruction, and geologic evolution: Boulder, Colorado, Geological Society of America Memoir 178, p. 217–230.

Remeika, P., and Beske-Diehl, S., 1996, Magnetostratigraphy of the western Borrego Badlands, Anza-Borrego Desert State Park, California: Implications for stratigraphic age control, *in* Abbott, P.L., and Seymour, D.C., eds., Sturzstroms and detachment faults, Anza-Borrego Desert State Park, California: South Coast Geological Society Annual Field Trip Guidebook, no. 24, p. 209–220.

Retallack, G.J., 1990, Soils of the past: Boston, Massachusetts, Unwin Hyman, 520 p.

Revenaugh, J., 1998, Seismic estimation of cumulative offset on the San Jacinto fault zone: Eos (Transactions, American Geophysical Union), v. 79, p. F593.

Rockwell, T., Loughman, C., Merifield, P., 1990, late Quaternary rate of slip along the San Jacinto fault zone near Anza, Southern California: Journal of Geophysical Research, v. 95, p. 8593–8605.

Ryter, D.W., and Dorsey, R.J., 2000, Quaternary tectonic evolution of the central San Jacinto fault zone, southern California: Geological Society of America Abstracts with Programs, v. 34, no. 5, p. 86.

Sanders, C., and Magistrale, H., 1997, Segmentation of the northern San Jacinto fault zone, Southern California: Journal of Geophysical Research, v. 102, p. 27 453–27 467.

Sanders, C.O., 1989, Fault segmentation and earthquake occurrence in the strike-slip San Jacinto fault zone, California, *in* Schwartz, D.P., and Sibson, R.H., eds., Proceedings of Conference XLV, Workshop on fault segmentation and controls of rupture initiation and termination: U.S. Geological Survey Open-File Report, OF 89-0315, p. 324–349.

Sarna-Wojcicki, A.M., Bowman, H.W., Meyer, C.E., Russell, P.C., Asaro, F., Michael, H., Rowe, J.J., Baedecker, P.A., and McCoy, G., 1980, Chemical analyses, correlations, and ages of late Cenozoic tephra units of East-central and southern California: U.S. Geological Survey Open File Report, OF 80-231, 57 p.

Sarna-Wojcicki, A.M., Meyer, C.E., and Wan, E., 1997, Age and correlation of tephra layers, position of the Matuyama-Brunhes chron boundary, and effects of Bishop Ash eruption on Owens Lake, as determined from drill hole OL-92, southeast California, *in* Smith, G.I., and Bischoff, J.L., eds., An 800,000-year paleoclimatic record from core OL-92, Owens Lake, southeast California: Boulder, Colorado, Geological Society of America Special Paper, v. 317, p. 79–90.

Sarna-Wojcicki, A.M., Pringle, M.S., and Wijbrans, J., 2000, New $^{40}Ar/^{39}Ar$ age of the Bishop Tuff from multiple sites and sediment rate calibration for the Matuyama-Brunhes boundary: Journal of Geophysical Research, v. 105, p. 21 431–21 443.

Sharp, R.V., 1967, San Jacinto fault zone in the Peninsular Ranges of Southern California: Geological Society of America Bulletin, v. 78, p. 705–729.

Sharp, R.V., 1975, En echelon fault patterns of the San Jacinto fault zone, *in* Crowell, J.C., ed., San Andreas fault in southern California: A guide to San Andreas fault from Mexico to Carrizo Plain: Sacramento, California, Special Report, California Division of Mines and Geology, v. 118, p. 147–152.

Sharp, R.V., 1981, Variable rates of late Quaternary strike slip on the San Jacinto fault zone, Southern California, Journal of Geophysical Research, v. 86, p. 1754–1762.

Walker, R.G., and Cant, D.J., 1984, Sandy fluvial systems, *in* Walker, R.G., ed., Facies models: Waterloo, Geoscience Canada Reprint Series (2nd Edition), p. 71–89.

Weldon, R.J., and Humphreys, E., 1986, A kinematic model of southern California: Tectonics, v. 5, p. 33–48.

Weldon, R.J., and Sieh, K.E., 1985, Holocene rate of slip and tentative recurrence interval for large earthquakes on the San Andreas fault, Cajon Pass, southern California: Geological Society of America Bulletin, v. 96, p. 793–812.

Wells, D.L., 1987, Geology of the eastern San Felipe Hills, Imperial Valley, California: Implications for wrench faulting in the southern San Jacinto fault zone [M.Sc. thesis]: San Diego, California, San Diego State University, 140 p.

Wesnousky, S.G., 1986, Earthquakes, Quaternary faults, and seismic hazard in California: Journal of Geophysical Research, v. 91, p. 12 587–12 631.

Wesnousky, S.G., 1988, Seismological and structural evolution of strike-slip faults: Nature, v. 335, p. 340–343.

Zhang, P., Burchfiel, B.C., Chen S., Deng Q., 1989, Extinction of pull-apart basins: Geology, v. 17, p. 814–817.

MANUSCRIPT ACCEPTED BY THE SOCIETY FEBRUARY 8, 2002

Printed in the U.S.A.